

1 **Automatic building information model reconstruction in high-density urban areas:**
2 **Augmenting multi-source data with architectural knowledge**

3 Ke Chen¹, Weisheng Lu², Fan Xue³, Pingbo Tang⁴, and Ling Hin Li⁵

4 ¹ Post-doctoral Fellow, Department of Real Estate and Construction, Faculty of Architecture, The
5 University of Hong Kong, Hong Kong, leochen@connect.hku.hk;

6 ² Associate Professor, Department of Real Estate and Construction, Faculty of Architecture, The
7 University of Hong Kong, Hong Kong, wilsonlu@hku.hk;

8 ³ Research Assistant Professor, Department of Real Estate and Construction, Faculty of Architecture,
9 The University of Hong Kong, Hong Kong, xuef@hku.hk;

10 ⁴ Assistant Professor, Del E. Webb School of Construction, Arizona State University, USA,
11 tangpingbo@asu.edu;

12 ⁵ Associate Professor, Department of Real Estate and Construction, Faculty of Architecture, The
13 University of Hong Kong, Hong Kong, lhli@hku.hk;

14

15 **Abstract:** Many studies have been conducted to create building information models (BIMs) or
16 city information models (CIMs) as the digital infrastructure to support various smart city
17 programs. However, automatic generation of such models for high-density (HD) urban areas
18 remains a challenge owing to (a) complex topographic conditions and noisy data irrelevant to
19 the buildings, and (b) exponentially growing computational complexity when the task is
20 reconstructing hundreds of buildings at an urban scale. This paper develops a method — multi-
21 Source recTification of gEometric Primitives (mSTEP) — for automatic reconstruction of
22 BIMs in HD urban areas. By retrieving building base, height, and footprint geodata from
23 topographic maps, level of detail 1 (LoD1) BIMs representing buildings with flat roof
24 configuration were first constructed. Geometric primitives were then detected from LiDAR
25 point clouds and rectified using architectural knowledge about building geometries (*e.g.* a
26 rooftop object would normally be in parallel with the outer edge of the roof). Finally, the
27 rectified primitives were used to refine the LoD1 BIMs to LoD2, which show detailed
28 geometric features of roofs and rooftop objects. A total of 1,361 buildings located in a four
29 square kilometer area of Hong Kong Island were selected as the subjects for this study. The
30 evaluation results show that mSTEP is an efficient BIM reconstruction method that can
31 significantly improve the level of automation and decrease the computation time. mSTEP is
32 also well applicable to point clouds of various densities. The research is thus of profound
33 significance; other cities and districts around the world can easily adopt mSTEP to reconstruct
34 their own BIMs/CIMs to support their smart city programs.

35

36 **Keywords:** building information model; city information model; LiDAR point clouds;
37 topographic map; architecture; high-density city

38

39 **1. Introduction**

40 City reconstruction in 3D digital format emerges popularity in the era of information (Heo *et*
41 *al.* 2013). A city information model (CIM) contains spatial data and virtual representations of
42 all objects of interest in an urban area. A well-developed CIM can facilitate the work of city
43 planners and urban designers in addressing urban problems such as traffic congestion,
44 accessibility, connectivity, and the potential impact of natural disasters (AECbytes 2016). From
45 a city administrator's perspective, a CIM with rich information can be useful for city
46 governance, while at the individual citizen level, a CIM enables applications such as
47 transportation navigation, emergency response, and many other location-based services. Cities
48 such as New York, London, Berlin, and Adelaide have all created their CIMs to support many
49 of the applications cited above (Over *et al.* 2010; Gröger and Plümer 2012; Sun and Salvaggio
50 2013).

51

52 Buildings are the most important manmade objects in the urban scene (Henricsson and
53 Baltsavias, 1997). Many studies, over the years, have focused on the reconstruction of building
54 information models (BIMs) (*e.g.* Tang *et al.* 2010; Xue *et al.* 2018) which can be stitched
55 together to form a CIM. Another approach is to create CIMs using Geographic Information
56 Systems (GIS) (Li *et al.* 2015) and remote sensing (Haala and Kada 2010; Lillesand *et al.* 2015).
57 In these CIMs, individual buildings could be roughly represented by prisms or "boxes" without
58 precise information on the "as-is" condition. With the advancements of data acquisition and
59 processing technologies, the trend is to reconstruct BIMs that contain detailed geometric
60 features of roofs and rooftop objects (so termed as Level of Detail 2 [LoD2] defined by the
61 Open Geospatial Consortium [OGC] [2012]) to extend CIM applications, *e.g.* green roof
62 development (Choi *et al.* 2017) and energy performance improvement (Yang and Zou 2016).
63 However, the reconstruction of BIMs, particularly those with greater details, is labor-intensive,
64 time-consuming, and error-prone (Volk *et al.* 2014). The process requires a considerable
65 amount of manual rectifications and computational power, and this becomes extreme
66 burdensome when the task is at the urban scale (Sun and Salvaggio 2013; Li *et al.* 2016; Wu
67 *et al.* 2017).

68

69 Researchers have attempted to improve the efficiency of BIM reconstruction by introducing
70 automatic or semi-automatic approaches. Images, 3D laser scanning point clouds, and total
71 station surveying data are commonly used for model reconstruction (*e.g.* Awrangjeb *et al.* 2013;
72 Li *et al.* 2016; Wu *et al.* 2017). Algorithms have been developed to process different types of

73 data and reconstruct BIMs (*e.g.* Heo *et al.* 2013; Xue *et al.* 2018). In addition, with data from
74 multiple sources become affordable, it is now possible to use multi-source data to overcome
75 some of the inherent problems (*e.g.* inaccurate/"noisy" data, incomplete information)
76 associated with single-source data (*e.g.* Habib *et al.* 2010; Cheng *et al.* 2011; Gilani *et al.*
77 2016). Acknowledging considerable achievements in the field of BIM/CIM reconstruction,
78 BIM/CIM reconstruction in high-density (HD) urban areas remains an open problem
79 (Musialski *et al.* 2013). Firstly, city features such as trees, roads, and terrain introduce a lot of
80 noise that undermines the quality of the measurement data. Secondly, densely-distributed
81 buildings make it difficult to segment data for generating individual BIMs. Lastly,
82 reconstructing thousands of buildings at an urban scale exponentially increases the
83 computational complexity, bringing many difficulties for methods which rely on general object
84 recognition approaches to derive geometric primitives to form the building models.

85

86 This study aims to improve automatic BIM reconstruction in HD urban areas by proposing a
87 reconstruction method called multi-Source recTification of gEometric Primitives (mSTEP).
88 mSTEP harnesses the data from multiple sources and makes use of architectural features (*e.g.*
89 parallels and symmetries) to reduce the noisy data and fine-tune the geometric primitives to
90 reconstruct LoD2 BIMs automatically. The data employed in this study comes from the Hong
91 Kong governmental agencies, comprising digital topographic map and light detection and
92 ranging (LiDAR) point cloud. Given the fact that such types of data are extensively available
93 in many cities and districts around the world, mSTEP can be applied to reconstruct their
94 BIMs/CIMs in an efficient manner.

95

96 The organization of the paper is as follows: Section 2 reviews the state-of-the-art studies on
97 BIM reconstruction. Section 3 describes the overall research progress, the subject area and
98 characteristics of the corresponding topographic map and LiDAR point clouds. Section 4
99 details the BIM reconstruction method – mSTEP. Section 5 provides a comprehensive
100 discussion of the evaluation results, discusses the parameter configuration of mSTEP, and
101 shows the compatibility of mSTEP with a denser point cloud. Section 6 concludes with a
102 summary and highlights future research directions.

103

104 **2. Literature Review**

105 Previous studies on the generation of BIMs in the urban environment can be viewed from two
106 different perspectives: (1) The raw data used for BIM reconstruction; and (2) the methods

107 employed in processing the data. While the two perspectives are related, the discussion deals
108 with each perspective separately for the sake of clarity.

109

110 **2.1 Original datasets**

111 Aerial and satellite images are typical data sources for large-scale BIM reconstruction.
112 Spaceborne sensors like IKONOS, QuickBird, and GeoEye-1 have provided 1m-resolution
113 satellite images for 3D building reconstruction (Lafarge *et al.* 2008; Poli *et al.* 2015). Aerial
114 image resolution can be even higher than that of satellite images, in some cases, reaching
115 decimeter accuracy. Owing to their high image resolution as well as the widespread use of
116 unmanned aerial vehicles (UAVs), the uses of aerial images to create 3D models of individual
117 buildings or even to reconstruct the entire urban scenes are increasing (Li *et al.* 2016).

118

119 LiDAR point clouds have also been widely used for BIM reconstruction. It typically utilizes
120 laser light which is projected on surfaces and its reflected backscattering is captured for
121 generating 3D point clouds. Heo *et al.* (2013) used LiDAR point clouds to develop the models
122 of 29 buildings. Other studies including Sun and Salvaggio (2013), Xiong *et al.* (2014), and
123 Yan *et al.* (2016) used airborne LiDAR point clouds to model a limited number of buildings
124 with roofs of various shapes. With the availability of city-scale LiDAR point clouds, Poullis
125 and You (2009) created simplified BIMs within a large city area.

126

127 Topographic maps, which describe urban objects in terms of geometry, land use, and other
128 attributes, are another important data source for BIM reconstruction at city- or district-scale. In
129 addition to the topographic maps produced by government agencies, recent years have seen the
130 emergence of open-access geographic datasets. For example, OpenStreetMap (OSM) – a
131 prominent volunteered geographic information service – has been used for BIM reconstruction
132 (Over *et al.* 2010). However, without official verification, the common problem of open-access
133 geographic datasets is their completeness and accuracy.

134

135 The use of single-source data for BIM reconstruction, be it aerial images or LiDAR point
136 clouds, is prevailing but still poses problems such as “noisy” data caused by complex urban
137 features and incomplete information (Cheng *et al.* 2011). These drawbacks have given rise to
138 increased use of multi-source data for BIM reconstruction. A number of studies have confirmed
139 that using multi-source data can overcome some of the problems associated with the use of

140 single-source data (Rottensteiner and Jansa 2002; Alexandar *et al.* 2009; You and Lin 2011;
141 Henn *et al.* 2013; Zhang *et al.* 2014; Zhu *et al.* 2015).

142

143 **2.2 Data processing methods**

144 Various data processing methods have been proposed for BIM/CIM reconstruction (Haala and
145 Kada 2010; Musialski *et al.* 2013). Aerial or satellite images can be processed into digital
146 elevation model (DEM) (Lafarge *et al.* 2008; Poli *et al.* 2015) from which building models can
147 be extracted by applying height thresholds. With the further development of image matching,
148 an alternative way is to generate colored point clouds from a number of aligned aerial images
149 and then processed the generated point clouds into textured BIMs, which are formed by a large
150 number of small geometric primitives (Singh *et al.* 2014). This method, however, requires
151 careful selection of images and manual interpretation to adjust the building models is often
152 needed. Li *et al.* (2016) also generated point clouds from images, and proposed an object-level
153 point cloud segmentation and roof extraction. However, their method was only tested on
154 buildings with flat roofs.

155

156 Processing LiDAR data starts with segmentation of the point clouds of individual buildings.
157 This can generally be achieved using semantic segmentation approach (Lin *et al.* 2013),
158 classification or clustering algorithms (Zhu *et al.* 2015; Cao *et al.* 2017) or the reflectance value
159 captured by the LiDAR sensors (Sun and Salvaggio 2013). LiDAR point clouds can also be
160 integrated with other datasets. For example, building footprints retrieved from a topographic
161 map can provide a reference for segmenting the point clouds of buildings (Alexander *et al.*
162 2009; Ledoux and Meijers 2011). The segmentation of LiDAR point clouds can also be
163 improved with aerial images that provide regions of homogeneous gray level or color
164 distribution (Rottensteiner and Jansa 2002). Once segmented, the point clouds are used to
165 model the buildings with roofs and rooftop objects by various methods. A typical method is to
166 decompose the roof shapes into simple pre-defined ones by 2D plans (Henn *et al.* 2013) or
167 graph matching technique (Xiong *et al.* 2014), but the reconstruction may fail if the roof shape
168 is not pre-defined in the model library. Connecting the extracted primitives to form the roof
169 features is also widely-used due to its flexibility (Poullis and You 2009; Zhang *et al.* 2014; Yan
170 *et al.* 2016). However, such kind of method is sensitive to noise (Goebbelsa and Pohle-
171 Fröhlich 2016) and so far have only been used for specific roof forms.

172

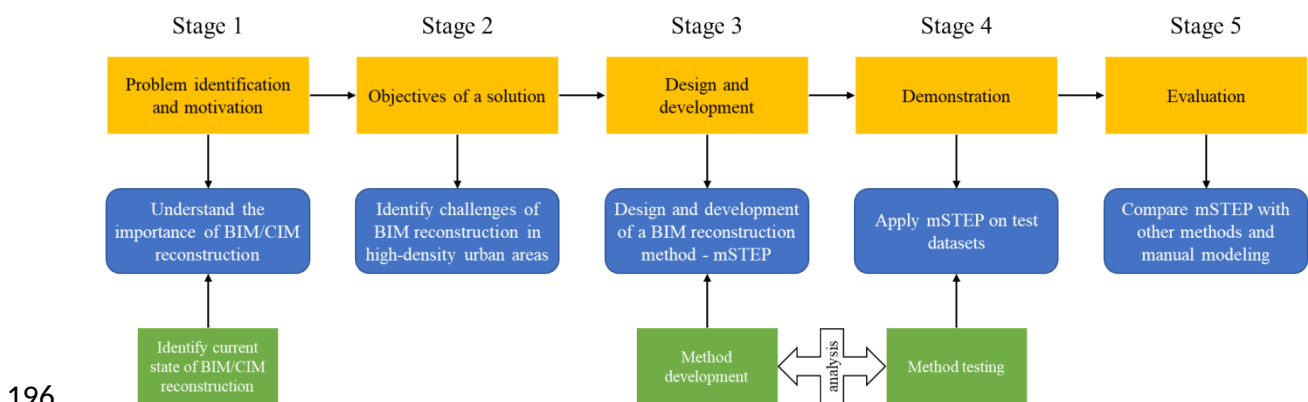
173 Although it is difficult to directly compare all these reconstruction methods since they are
 174 developed under different context with their own emphasis, our review has revealed that
 175 existing data processing methods usually require much time for noise filtering and assume
 176 buildings with flat or other simplified roof structures. Those methods that can generate more
 177 differentiated building and roof structures require considerable manual interpretation for pre-
 178 or post-processing. Actually, architectural designs commonly exhibit some conventional
 179 features such as parallels, symmetries or other structural regularities, which are not accidental,
 180 but often the result of economical, manufacturing, functional, or aesthetic considerations (Mitra
 181 and Pauly 2008). Parallel and perpendicular features have been used as the constraints to
 182 segment the point cloud to extract planar segments that constitute approximate building roof
 183 structure (Dorninger and Pfeifer 2008, Sampath and Shan 2010). However, few studies have
 184 systematically applied architectural rules to reconstructing BIMs of densely-distributed
 185 buildings in large-scale urban areas. As will be demonstrated in this study, rules derived from
 186 architectural conventions can help reduce the noise in the collected data and improve the
 187 efficiency of the modeling method and the informativeness of the reconstructed models.

188

189 3. Research approach

190 3.1 Overview of the research process

191 Given the aim of this study, a design science research approach (Peppers *et al.* 2008) is adopted
 192 to develop an automatic and efficient BIM reconstruction method. Design science focuses on
 193 not only understanding problems, but also developing methods or artifacts with the explicit
 194 intention of improving human performance (Van Aken 2005). A diagrammatic illustration of
 195 the research process is presented in Figure 1.



196

197 Figure 1 Research process

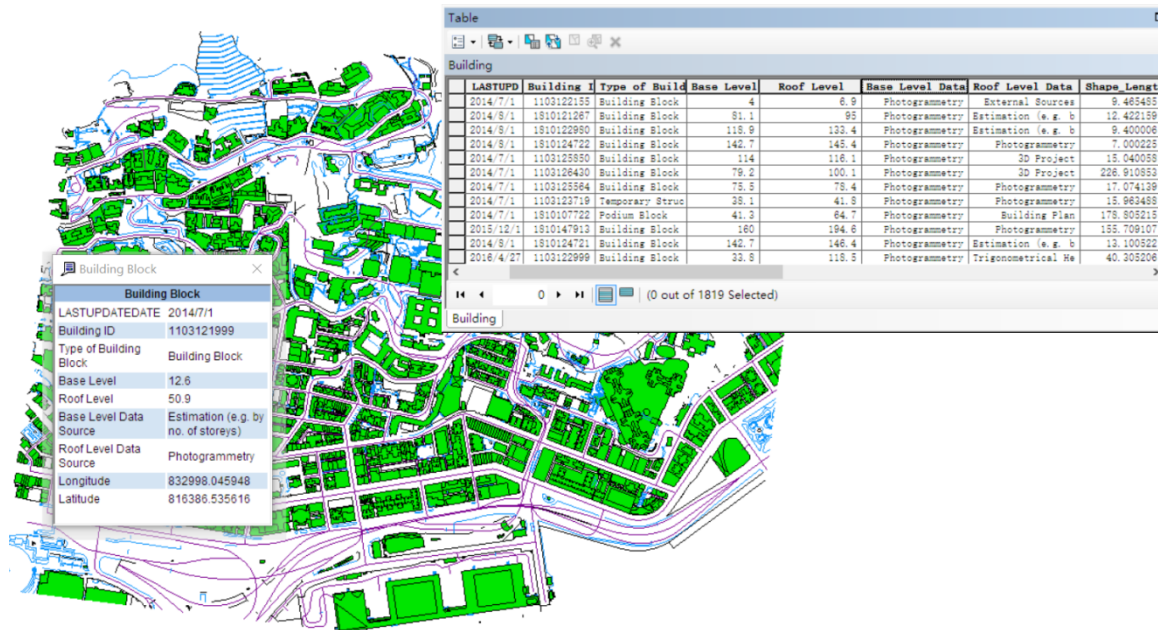
198

199 By identifying the challenges of BIM reconstruction in high-density urban areas, multi-Source
200 recTification of gEometric Primitives (mSTEP) was proposed, which takes the topographic
201 map, point clouds, and architectural conventions as inputs and generates BIMs with detailed
202 rooftop structures and objects identified. A 2km×2km area in northwestern Hong Kong Island,
203 containing 1,361 blocks of densely-distributed buildings of varying heights and shapes, was
204 selected as the subject area since all identified challenges of BIM reconstruction exist in this
205 area: The buildings are surrounded by urban features like trees on hills and slopes, commercial
206 signs and power lines, which create noise in the data captured for BIM reconstruction; The
207 narrow gaps between buildings also cause severe occlusions in the collected data. In
208 combination, these factors present difficulties for segmentation, refinement and other BIM
209 reconstruction processes. After applying mSTEP on test datasets, the generated BIMs were
210 compared with results from another two reconstruction methods (*i.e.* methods described in
211 Javanmardi et al. [2015] and Wu et al. [2017]) and manual modeling for evaluation.

212

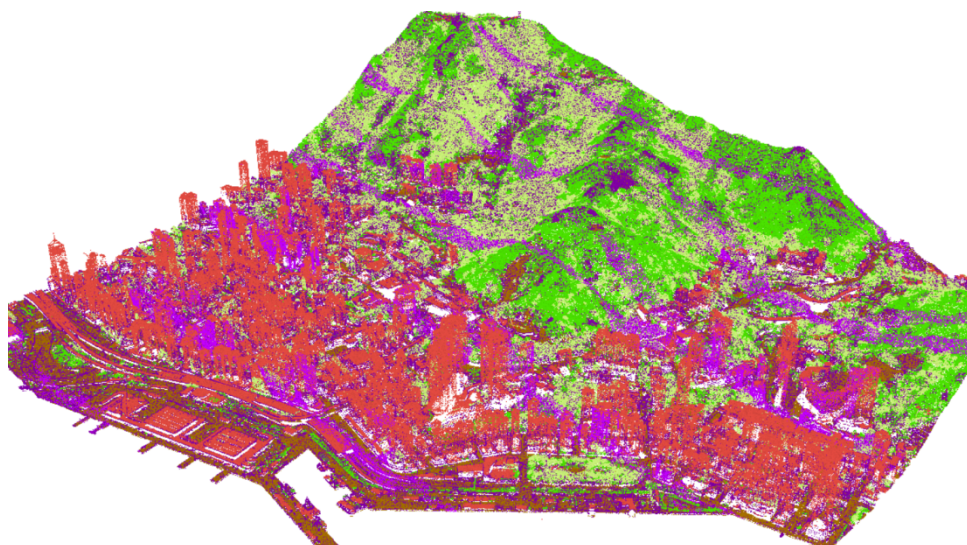
213 **3.2 Test datasets**

214 The topographic map used in this study was purchased from the Lands Department (LD) of
215 HKSAR. It is in Geodatabase (GDB) format with a scale of 1:1000. The Hong Kong 1980 Grid
216 Coordinates provides the latitude and longitude of the map, and heights are in meters above
217 the Hong Kong Principal Datum. The topographic map contains feature datasets including
218 *buildings, land cover, transportation, etc.* As shown in Figure 2, the buildings in the selected
219 region are shown in green with their boundaries in black. The map also contains data on
220 building ID, shape, shape area, type of building block, base level, roof level, and data source.
221 A preliminary analysis of the base and roof levels found that the datasets in the topographic
222 map are collected from various sources such as building plans, photogrammetry, and
223 topographic survey. Data for the buildings was last updated in the period 1 July 2014 to 27
224 April 2016.



225
 226 Figure 2 Data of the topographic map of the subject area

227
 228 The LiDAR point clouds used in this study was provided by the Civil Engineering and
 229 Development Department (CEDD) of HKSAR. The data, comprising buildings, roads, and
 230 many other urban features, was collected between 1 December 2010 and 8 January 2011 by
 231 the CEDD by hiring an airborne LiDAR surveying company. In the original dataset, the point
 232 density is about 4 points/m². Points classified according to American Society for
 233 Photogrammetry and Remote Sensing (ASPRS) laser (LAS) format specification 1.1 (ASPRS
 234 2005) are shown in different colors (see Figure 3). The classification codes represent the type
 235 of object that has reflected the laser pulse.

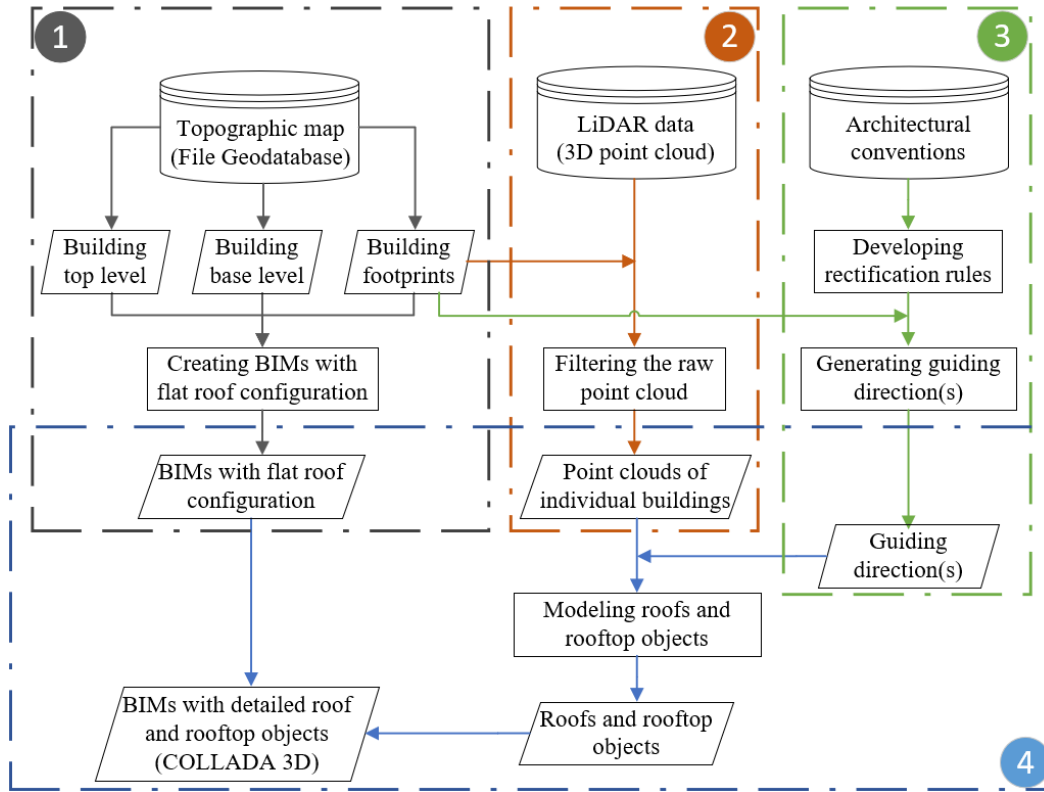


236
 237 Figure 3 An illustration of the LiDAR point clouds

238

239 **4. BIM reconstruction method**

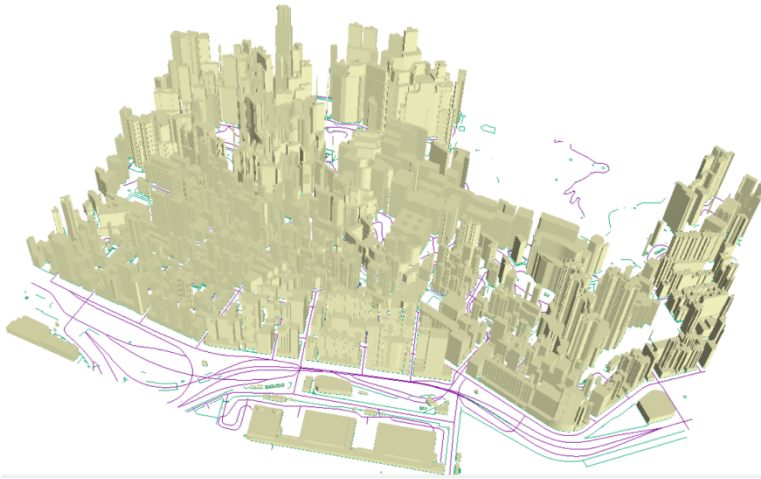
240 The main purpose of the proposed method — multi-Source recTification of gEometric
 241 Primitives (mSTEP) — is to enable automatic and efficient BIM reconstruction. The overall
 242 procedure of mSTEP is shown in Figure 4, which consists of four main phases. In this section,
 243 each of the four phases of mSTEP is introduced in details.



244
 245 Figure 4 Overall procedure of mSTEP

246
 247 **4.1 Reconstructing LoD1 BIMs from topographic map**

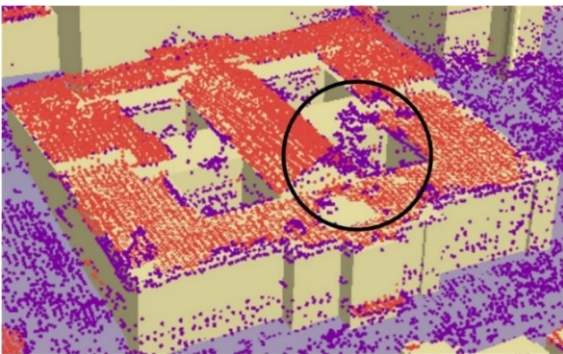
248 In the first phase, data in the topographic map is filtered to retrieve the data of building footprint,
 249 base level, and top level. By vertically stretching the footprint of each building according to
 250 the base level and top level of that building, the LoD1 BIM with flat roof configuration can be
 251 created (see Figure 5).



252
 253 Figure 5 An illustration of created LoD1 BIMs

254
 255 **4.2 Filtering the LiDAR point clouds**

256 The LiDAR point clouds is first filtered in *ESRI ArcScene* by using the classification codes to
 257 separate building point clouds from those of trees, terrain, and other features (ESRI 2016).
 258 However, it was found that many points of building structures were unclassified (see the circled
 259 area in Figure 6). Therefore, points classified as either “building” or “unclassified” were thus
 260 kept for further rectifications and other points were removed. Then, the point cloud of
 261 individual buildings was obtained by segmentation, a process accelerated through the use of
 262 building footprints contained in the topographic map. After converting the LiDAR point clouds
 263 and topographic map in the same coordinate system, points with XY-coordinates falling into
 264 the area zoned by a building footprint was segmented to that building.



265
 266 Figure 6 An example of unclassified points in the raw LiDAR point clouds

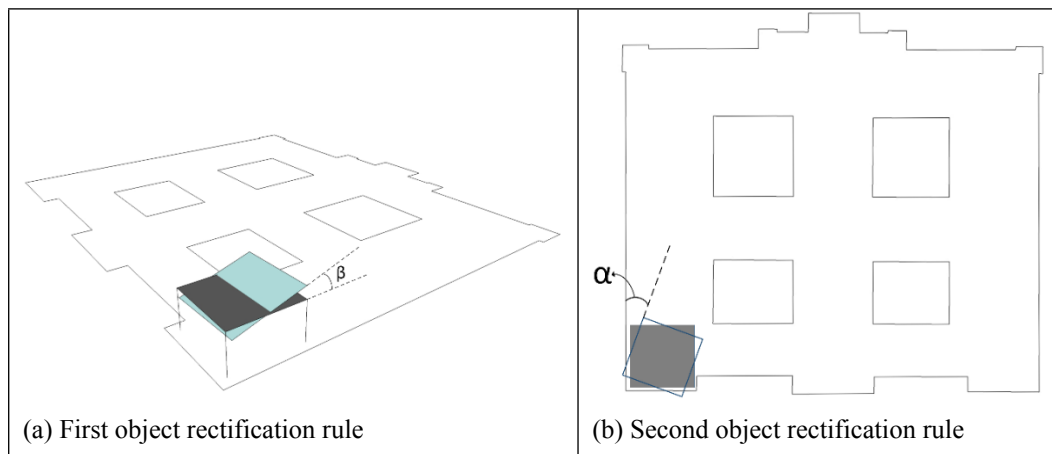
267
 268 **4.3 Developing object rectification rules from conventional architectural features**

269 Architectural conventions refer to the domain knowledge applied in the architectural design,
 270 such as geometrical or physical features (*e.g.* flatness, parallels, and symmetries) of building
 271 objects and their spatial relationships (Cantzler 2003). Some of the conventions can be obtained

272 from ordinances or standards, while others can be originated from general observation in real-
273 world situations. In this study, two object rectification rules are developed based on very simple
274 architectural conventions to ensure “structural regularity”: (1) the top surface of rooftop objects
275 are either in parallel with the horizontal plane or with a considerable angle of dip; and (2) the
276 rooftop objects are normally in parallel with the outer edge of roof.

277

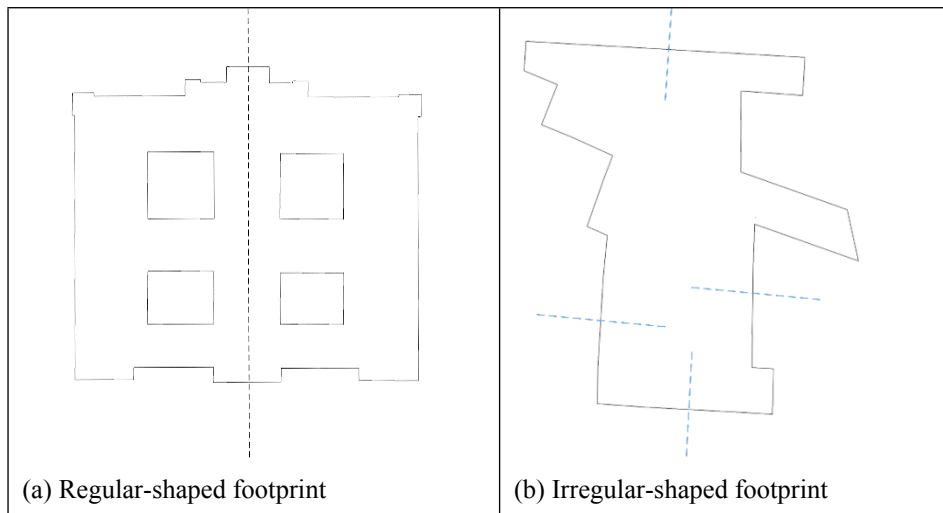
278 Both rules should be satisfied when rectifying the geometric primitives detected from the
279 segmented LiDAR point clouds to form roofs and rooftop objects. An illustration of
280 rectification by the first rule is presented in Figure 7(a). The rectangle in blue is the top surface
281 of a rooftop object, which has a very small angle β of dip to the horizontal plane (*i.e.* the roof).
282 Therefore, this detected primitive is against the first rule, and should be rotated to be the
283 rectangle in gray, which is in parallel with the horizontal plane. An illustration of rectification
284 by the second architectural rule is shown in Figure 7(b). The rectangle in dashed line is not in
285 parallel with the outer edge of the roof, but has a deviation of angle α . This is rare in
286 architectural conventions, therefore, it should be rotated to be the rectangle in gray.



287 Figure 7 An illustration of the two rules of rectification

288

289 In order to enable automatic application of these two rules, especially the second one, guiding
290 directions were derived from the building footprints since the outer edge of the roof and
291 building footprint usually have the same shape, unless it is an irregular-shaped building. As
292 can be seen in Figures 8(a) and (b), for simple, regular-shaped building footprint, its centerline
293 provide the guiding direction for the rooftop object to be in parallel with, while for irregular-
294 shaped building footprint, the centerlines of its top 25% longest lines will provide guiding
295 directions for the computer to check whether the rooftop object is in parallel with at least one
296 of the directions.



297 Figure 8 An illustration of deriving guiding direction(s) from building footprints

298

299 **4.4 Reconstructing LoD2 BIM by using object rectification rules**

300 In the last phase of mSTEP, LoD2 BIM is developed by using the two object rectification rules.

301 The pseudo code of this process is shown in Figure 9. Given a target building, its LoD1 model
 302 is inherited from the topographic map (Line 6). A variant of RANSAC (Fischler and Bolles
 303 1981; Schnabel *et al.* 2007) is adopted for detecting geometric primitives from LiDAR point
 304 cloud of the building rooftop (Lines 7-8). The application of RANSAC requires a set of
 305 parameters to be determined (see Table 1). Different values of these parameters have been
 306 tested in order to find the optimal parameter set regarding the LiDAR point clouds to be
 307 processed. It is decided to set *minimum number of support points* to 10, *maximum distance to*
 308 *primitive* to 0.02m, and *sampling resolution* to 1.0. *Maximum normal deviation* and
 309 *overlooking probability*, are set to 25° and 1.0×10^{-6} respectively. More details regarding the
 310 parameters configuration are provided in Section 5.2.

311

312 Then, the detected geometric primitives are rectified to form the building roofs and rooftop
 313 objects. A tolerance level (ϵ), which is set to 0.05π , is used to determine whether one primitive
 314 needs rectification or not. The detected geometric primitives of roofs and rooftop objects will
 315 be rectified by the horizontal plane (Lines 9-13) and the guiding directions (Lines 14-21). After
 316 rectification, the volumetric models of roofs and rooftop objects can be created by projection
 317 to the top level of individual buildings, and will be integrated with the LoD1 BIMs created in
 318 the first phase to enrich them into LoD2 ones that have differentiated roof structures with higher
 319 completeness and accuracy (Lines 22-24).

```

2   input: a set of building exterior data sources ( $S$ ) of a building, including data in topographic map and
        LiDAR point clouds,
3       five parameters ( $param$ ) of RANSAC,
4       a tolerance level ( $\varepsilon$ ) for orientation rectification (default value of  $0.05\pi$ )
5   output: an LoD2 building model ( $M$ ) with detailed roof and rooftop objects
6    $M \leftarrow$  a LoD1 model from topographic map ( $S$ )           //referring to subsection 4.1
7    $r \leftarrow$  filter point cloud of rooftops ( $S$ );           //referring to subsection 4.2
8    $P \leftarrow$  RANSAC ( $r, param$ );                             //detecting geometric primitives
9   loop for each  $p$  in  $P$                                      //for each detected geometric primitive
10       $\alpha \leftarrow$  heading of normal ( $p$ );  $\beta \leftarrow$  dip of plane ( $p$ ); // for  $\alpha$  and  $\beta$  referring to Figure 7
11      if  $|\beta| < \varepsilon$  or  $|\pi - \beta| < \varepsilon$            //if  $\beta$  is close to the horizontal plane
12          $\beta \leftarrow 0$                                      //rectify w.r.t. the horizontal plane (as shown in Figure 7[a])
13      end if
14       $A \leftarrow$  derived guiding directions;
15      loop for each  $\alpha^*$  in  $A$                                //for each direction  $\alpha^*$ 
16         loop for  $q = -2$  to  $2$                                //for each quadrant
17            if  $|\alpha - \alpha^* + q \times \pi / 2| < \varepsilon$  //if  $\alpha$  is close to  $\alpha^*$ 
18                $\alpha \leftarrow \alpha^* - q \times \pi / 2$  //rectify w.r.t. the direction  $\alpha^*$  (as shown in Figure 7[b])
19            end if
20         end loop
21      end loop
22      if  $\alpha, \beta$  meets the two object rectification rules
23          $M \leftarrow M \cup$  update and 3D projection( $p, \alpha, \beta$ ) //enrich LoD1 BIM with roof and rooftop objects
24      end if
25  end loop
26  return  $M$ 

```

320 Figure 9 Pseudo code of the multi-source rectification

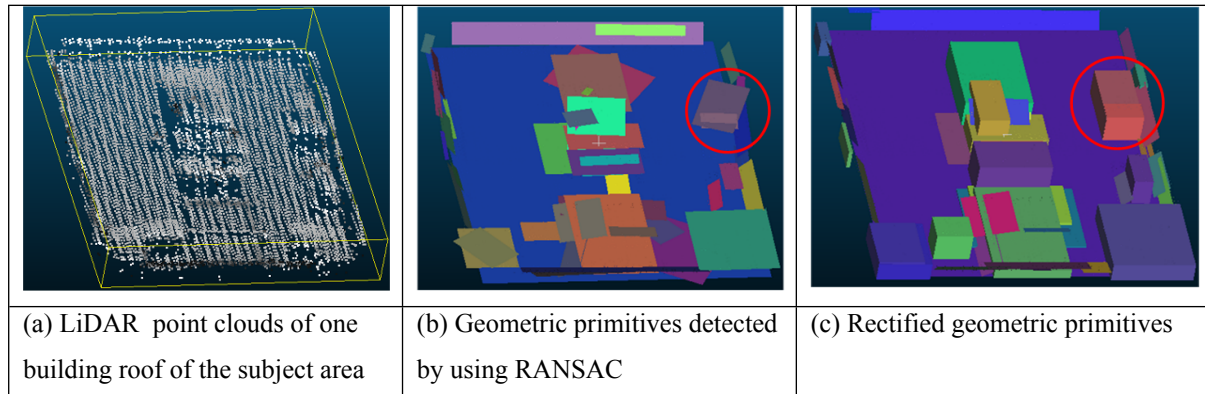
321

322 Table 1 Descriptions of the RANSAC parameters

Parameter	Description
minimum number of support points	The minimum number of points required to identify a geometry. A larger <i>minimum support points</i> means a more rigorous geometry detection process.
maximum distance to primitive	The maximum distance of an inlier point to a geometry.
sampling resolution	The parameter determines the sample rate of neighboring points
maximum normal deviation	The difference between the normal at a point and the normal of a geometry at the closest project of that point onto that geometry.
overlooking probability	The parameter controls the population size of the primitive candidates.

323

324 A demonstration of multi-source rectification is shown in Figure 10. At the beginning,
 325 geometric primitives are detected from LiDAR point clouds (see Figure 10[a]) by RANSAC,
 326 but the detected geometric primitives may not be corrected from an architectural point of view.
 327 For instance, in Figure 10(b), the rectangle marked in red circle conjuncts to the roof surface
 328 at an angle. Then, the detected primitives are rectified according to the horizontal plane and
 329 the guiding direction(s). After that, the rectified primitives will be projected to create
 330 volumetric models of roofs and rooftop objects (see Figure 10[c]).



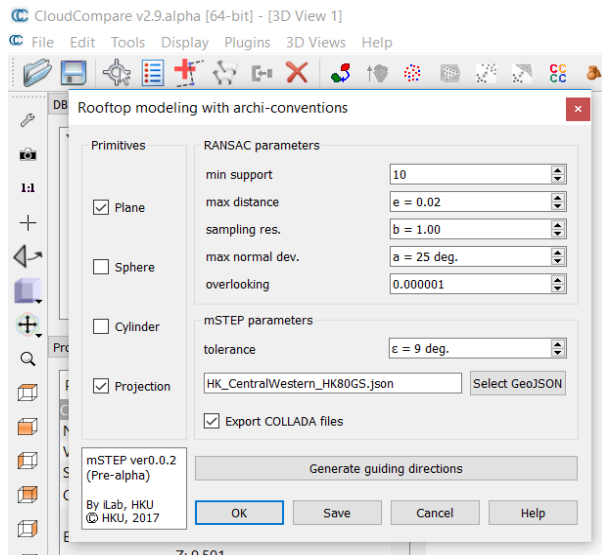
331 Figure 10 A demonstration of the multi-source rectification

332

333 5. Evaluation

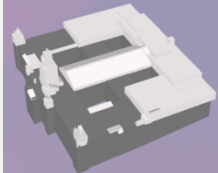

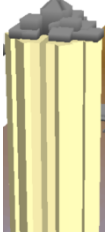

334 5.1 Overall results

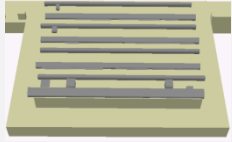




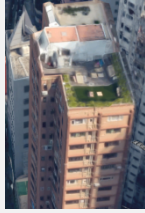
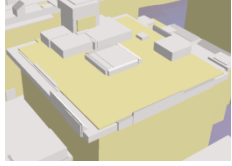
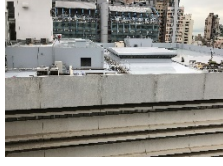
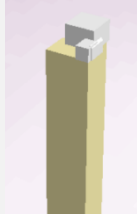

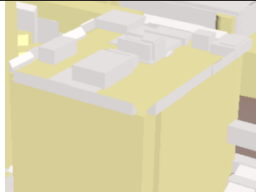

335 In this study, the first phase of mSTEP is performed in *ESRI ArcScene*, and the remaining three
 336 phases are automatically performed by using a plug-in of *CloudComapre* which is tailor-
 337 programmed in C++ by the authors. A screenshot of the plug-in is shown in Figure 11. The
 338 computation environment was a personal notebook with 2.6GHz Quad-core CPU, 16 GB RAM,
 339 and a 64-bit Microsoft Windows 10 operating system. Applying mSTEP, the automatic
 340 generation of BIMs in the subject area took 319.7 seconds. 81.9% of the 1,361 buildings were
 341 successfully modeled. Among the remainder, 113 buildings do not have either the base level
 342 or the roof level in the topographic map, and 134 buildings lacked points in the LiDAR dataset
 343 for modeling of the roofs and the rooftop objects.



344
 345 Figure 11 The screenshot of the developed *CloudCompare* plug-in
 346

347 Some examples of the reconstructed models are shown in Figure 12. Among the buildings
 348 shown include a building on a university campus (*ID: 11**374*), Edwardian Baroque in style
 349 with a central clock tower and several turrets; a residential building with a pyramid-shaped
 350 roof and many rooftop objects (*ID: 11**486*); a wholesale food market with a strip-shaped
 351 roof and several box-shaped air conditioners (*ID: 11**535*); and a residential building (*ID:*
 352 *11**845*) with flat roof and cuboid-shaped rooftop objects. Other building models shown in
 353 Figure 12 also have their roof and rooftop objects in the correct shapes constituted without the
 354 need for manual post-modifications. By manually checking the 3D building models and the
 355 actual buildings, it can be seen that the models reach the LoD2 that possess more detailed
 356 information than simple “boxes”. It can also be seen that the models are in an acceptable
 357 standard of accuracy.

Building ID in the topographic map	Reconstructed model (colors are for distinguishing only)	Photo (collected from the Internet or taken by the authors)
11**374		
11**486		

11**535		
11**845		
11**386		
11**200		
11**500		
11**345		

358 Figure 12 An illustration of the reconstructed models and actual buildings

359

360 5.1.1 Efficiency assessment

361 To assess the efficiency of reconstruction, the time spent on reconstructing buildings by using
362 mSTEP was compared with the time required for manual modeling. In *SketchUp*, two human
363 modelers, who have over four years' experience in architectural drawing, created LoD2 BIMs
364 based on base and roof levels from the topographic map and the segmented LiDAR point clouds.
365 They began modeling at the same time and alerted the researchers once they finished each of
366 the nine models so that the time they spent on modeling each building was recorded. In addition,
367 mSTEP was compared with: (1) a concave hull and Hough transform based reconstruction
368 method (take LiDAR point cloud and topographic map as inputs) introduced in Javanmardi et

369 al. (2015); and (2) a bipartite graphic matching-based reconstruction method introduced in Wu
 370 et al. (2017). The two reconstruction methods were selected for comparison due to two reasons.
 371 First, all the three methods share the same vision of enhancing 3D model reconstruction by
 372 taking advantage of architectural conventions and graph theory. The other reason was that their
 373 input point clouds were all airborne LiDAR data of HD urban areas. The comparison was based
 374 on three commonly-adopted metrics, including (1) *reconstruction time*; (2) *percentage of*
 375 *points that are segmented to support the detection of geometric primitives*; and (3) *root mean*
 376 *square error (RMSE) of the distances of points to their corresponding primitives*. The
 377 assessment results on nine randomly-selected buildings are presented in Table 2.

378 Table 2 Assessment results

No.	Number of points	mSTEP			Javanmardi et al. (2015) [†]			Wu et al. (2017) [‡]			Manual
		Time (s)	Segmented (%) [#]	RMSE (m) [*]	Time (s)	Segmented (%) [#]	RMSE (m) [*]	Time (s)	Segmented (%) [#]	RMSE (m) [*]	Time (In average; s)
1	270	0.03	75.2	0.114	0.02	63.1	0.119	0.01	88.3	0.341	266.65
2	372	0.03	77.7	0.048	0.01	58.7	0.157	0.01	60.4	0.223	171.23
3	620	0.40	87.6	0.065	0.02	84.7	0.098	0.01	78.8	0.370	94.33
4	2,491	0.16	48.6	0.196	0.05	31.6	0.199	0.01	99.8	0.315	2,486.75
5	2,682	0.09	90.0	0.057	0.03	60.2	0.049	0.01	89.6	0.251	515.65
6	7,212	0.23	91.1	0.067	0.04	26.4	0.067	0.01	90.4	0.280	597.92
7	8,987	0.26	85.1	0.065	0.09	18.8	0.097	0.01	100.0	0.257	1,386.16
8	24,878	2.23	86.3	0.068	0.13	66.2	0.163	0.02	99.1	0.340	2,498.84
9	29,506	0.47	90.1	0.088	0.21	71.1	0.230	0.02	99.9	0.291	701.43

379 [†]: The parameter β of Javanmardi et al. (2015)'s method was set to 0.5m as the average point distance;

380 [‡]: The two parameters, i.e., variable n and contour interval d_i , were set as 250 and 0.5m based on Wu et al.
 381 (2017)'s experimental results.

382 [#]: Percentage of points that are segmented to support the detection of geometric primitives.

383 ^{*}: Root mean square error of the distances of segmented points to their corresponding primitives.

384

385 The results in Table 2 showed that mSTEP achieved a competitive performance. Specifically,
 386 both mSTEP and Javanmardi et al. (2015)'s method reconstructed accurate geometric
 387 primitives for segmenting the point clouds. The proposed mSTEP segmented more points than
 388 Javanmardi et al. (2015)'s to support the detection of geometric primitives and reconstruct
 389 BIMs with less RMSE. In contrast, Wu et al. (2017)'s method achieved a fast reconstruction
 390 with a high-level of segmentation; yet at a significant cost of error (see the level of RMSE).
 391 The results confirmed that mSTEP could overcome the three identified challenges in BIM
 392 reconstruction in HD urban areas, i.e., much noise in measurement data, difficulties in
 393 segmenting data of densely-distributed buildings, and high computational complexity. With

394 the help of mSTEP, the efficiency of BIM reconstruction in HD urban areas can be
395 considerably improved.

396

397 Nevertheless, there seems no convincing way to measure the exact accuracy of the
398 reconstructed BIMs scientifically due to the lack of ground truth (Poullis and You 2009; Sun
399 and Salvaggio 2013). It is far from an effective measurement to reflect the resemblance
400 between the generated BIMs and the “as-is” condition. Neither can the model accuracy be
401 measured using a single index, such as the physical volume. A BIM professional, with expertise
402 and insights, can also tell whether the accuracy of a reconstructed 3D model is “acceptable” or
403 not. The issue of measurement standard is left for further studies.

404

405 ***5.1.2 Identified problems***

406 During application of mSTEP, it was found that the modeling outcomes can be affected by the
407 accuracy of data used, including the building footprints and heights in the topographic map,
408 and the LiDAR point clouds. Regarding the topographic map used in this study, some building
409 footprints were inaccurate and some heights were generated by estimation. This affected the
410 quality and accuracy of the retrieved guiding directions and, in turn, the accuracy of geometric
411 primitives detected from the point clouds.

412

413 Regarding the accuracy of the LiDAR point clouds, this is adversely affected by missing points
414 and interference caused by densely-distributed buildings, city features, and the like. mSTEP
415 can address interference, but not the problem of missing data. In this study, three factors
416 resulted in missing data. Firstly, the LiDAR scan pulse typically does not provide a detectable
417 return from transparent materials such as glass. Therefore, the points for roofs and rooftop
418 objects made of such materials were missing and thus could not be used for BIM reconstruction.
419 Secondly, the density of the point cloud was 4 points/m². This may not be sufficient to capture
420 data on certain rooftop objects, such as parapet walls that are relatively thin in the horizontal
421 dimension. Thirdly, the LiDAR point clouds, collected from 2010 and 2011, was not up-to-
422 date.

423

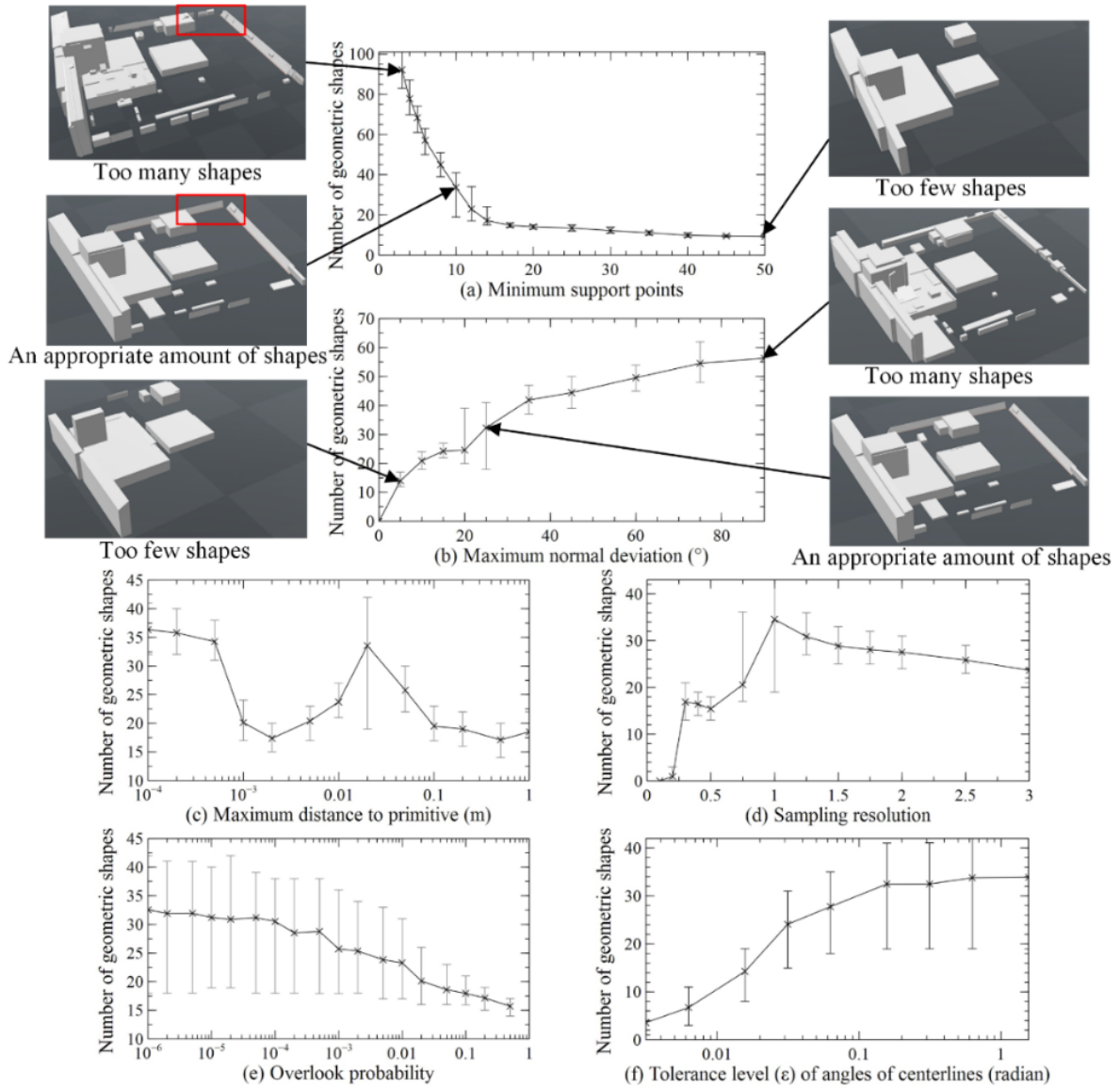
424 ***5.2 Parameter configuration of mSTEP***

425 A set of tests was performed on the parameter configuration of mSTEP. The purpose is to
426 identify the parameters that can significantly impact the modeling outcomes measured by the
427 *average number of detected geometric primitives*. This indicator is chosen because it measures

428 the primitives generated from the LiDAR point clouds to form the roof and rooftop objects.
429 Generally, the larger value the indicator, the more details the roof and rooftop objects have
430 been reconstructed by mSTEP. However, excessive primitives detected are also undesirable
431 since they are often caused by a single rooftop object being separated into several small pieces
432 (e.g. a pipe separated into different trunks), which actually decrease the accuracy of
433 reconstruction.

434

435 The parameters to be tested include the *tolerance level* and the five RANSAC parameters in
436 terms of (a) *minimum number of support points*, (b) *maximum normal deviation*, (c) *maximum*
437 *distance to primitive*, (d) *sampling resolution*, and (e) *overlook probability*. The test subject is
438 the LiDAR point clouds of a randomly-selected building, which has an *ID 11**200* in Figure
439 12. The tests aim at evaluating the sensitivity of each parameter, therefore when performing
440 the testing one parameter, other five parameters are controlled, *i.e.* remaining unchanged. In
441 the single factor sensitivity analysis, for each parameter, the tests were replicated for 100 times
442 to get the statistic values at 5th and the 95th percentiles. The results of all tests are shown in
443 Figure 13. In each of the six sub-figures, the Y-axis on the left denote the number of geometric
444 primitives detected by mSTEP, the X-axis denotes the value of the tested parameter. The box
445 chart shows the average values, and the 5th and the 95th percentiles of the indicator. The curve
446 depicted in each sub-figure illustrates the trend of value changes of the indicator as reflection
447 to the value change of the parameter under evaluation.



448

449 Figure 13 Testing results of parameter configuration of mSTEP

450

451 Based on the results shown in Figure 13, it can be confirmed that *minimum number of support*
 452 *points* and *maximum normal deviation* are the two parameters that have the most significant
 453 impact on the indicator of *average number of detected geometric primitives* since the curves
 454 shown in Figure 13(a) and (b) cover a much wider range in Y-axis than the curves in the other
 455 four figures. Particularly in Figure 13(a), when *minimum number of support*
 456 *points* increase from 3 to 10, the indicator decreases steeply from 95 to 33.6. Once *minimum number of support*
 457 *points* exceed 10, the indicator will continuously decrease, at a slower pace, to 9. From the
 458 three outputs of mSTEP when *minimum number of support points* equal to 3, 10 and 50
 459 respectively, it can be seen that some of the rooftop objects such as the parapet wall are divided
 460 into small pieces (see the comparison between the two parts marked in red rectangle of Figure

461 13[a]). When *minimum number of support points* is set to 3, too many primitives are detected.
462 By contrast, when *minimum number of support points* is set to 50, many details of rooftop
463 objects are missing. Setting *minimum number of support points* to 10 can generate an
464 appropriate output. In Figure 13(b), when *maximum normal deviation* increases from 0° to 90°,
465 the *average number of detected geometric primitives* increases from 0 to 55.4. Similar to the
466 evaluation on *minimum support points*, three outputs when *maximum normal deviation* equals
467 to 5°, 25°, and 90° are presented, from which, it is found that setting *maximum normal deviation*
468 to 5° and 90° lead to too few and too many detected primitives respectively. When *maximum*
469 *normal deviation* equals 25°, an appropriate amount of primitives can be detected.

470

471 For the remaining four parameters, the impact of *maximum distance to primitive* on the
472 indicator is relatively complex. As it increases from 1.0×10^{-4} m to 1.0m, the *average number*
473 *of detected geometric primitives* fluctuates (see Figure 13[c]). It seems that setting *maximum*
474 *distance to primitive* to either 1.0×10^{-4} m or 0.02m can deliver similar outputs in terms of
475 quantity, but it is found that when *maximum distance to primitive* equals to 1.0×10^{-4} m, most of
476 the detected primitives are too small, which shows a lack of accuracy. Therefore, 0.02m is the
477 more appropriate value for *maximum distance to primitive*. Additionally, when *tolerance level*
478 increases from 0.001π to 0.5π , the *average number of detected geometric primitives* increases
479 from 3.58 to 33.91. Such impact, however, becomes negligible after *tolerance level* reaches
480 0.05π (see Figure 13[f]). For *sampling resolution*, when it is either less than 1.0 or large than
481 1.25, the *average number of detected geometric primitives* will become less than 30, which
482 decreases the accuracy of the reconstructed roof and rooftop objects (see Figure 13[d]). Finally,
483 for *overlook probability*, its overall influence is less significant compared with the other five
484 parameters (see Figure 13[e]). Its values between 1.0×10^{-6} and 5×10^{-5} can detect an appropriate
485 amount of primitives, but the best output is identified when setting *overlook probability* to
486 1.0×10^{-6} .

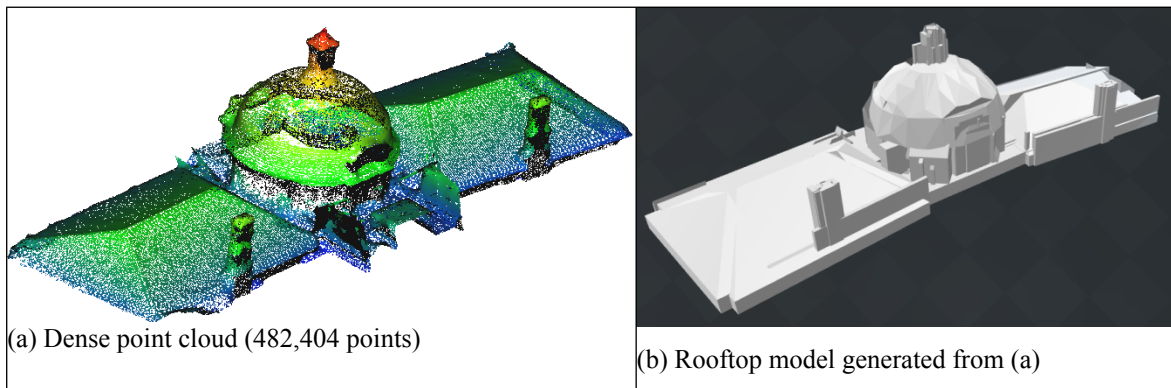
487

488 **5.3 Implementing mSTEP on dense point cloud**

489 The density of LiDAR point clouds used to reconstruct buildings in the subject areas is 4
490 points/m². With the improvement in sensing devices, the cost of data acquisition is expected to
491 continuously decrease and denser point clouds will become available. Therefore, it is necessary
492 to test the applicability of mSTEP to dense point clouds. Since few buildings in the subject area
493 have publicly available dense point cloud, a building at the main campus of the University of
494 Hong Kong in Hong Kong Island is selected for the test.

495

496 The dense point cloud of the selected building contains 482,404 points in total, which is
497 obtained by using SfM to process 200 photos taken by a UAV (see Figure 14[a]). Details about
498 SfM for processing images into point cloud can be found in Jancosek and Pajdla (2011). When
499 applying mSTEP to this dense point cloud, one parameter, i.e. *minimum number of support*
500 *points*, is changed from 10 to 30 in order to cope with the point density, while other five
501 parameters remain unchanged. The rooftop model is developed in 1.41s with 475 geometric
502 primitives detected (see Figure 14[b]). In doing so, mSTEP is proved to be capable of
503 reconstructing BIMs from a denser point cloud. A conclusion thus can be drawn that mSTEP
504 is applicable to both sparse point clouds (e.g. 4 points/m²) and dense point clouds for BIM
505 reconstruction. This suggests mSTEP can be applied to 3D building reconstruction in many
506 other cities or districts, which possess point clouds of various densities.



507 Figure 14 An illustration of applying mSTEP to a dense point cloud

508

509 6. Conclusions

510 The challenges of automatic reconstruction of building information models (BIMs)/city
511 information models (CIMs) in high-density (HD) urban areas are predominately twofold: (a)
512 the complex topographic conditions and noisy data, and (b) the heavy computational
513 complexity when the task is at an urban scale. This paper took the challenges by developing an
514 improved method — multi-Source recTification of gEometric Primitives (mSTEP) — for
515 automatic BIM reconstruction in complex urban areas. mSTEP comprises of several
516 interconnected steps to make good use of multi-source data including light detection and
517 ranging (LiDAR) point clouds, and topographic maps. The method has been validated through
518 a series of rigorous tests, and the results show that mSTEP is an efficient method to reconstruct
519 informative BIMs by significantly improving the level of automation and decreasing the
520 computation time.

521

522 Of particular originality of this research is augmenting the multi-source data with some simple
523 architectural conventions, which can effectively tackle the challenges of automatic BIM/CIM
524 reconstruction. Another original contribution made by this study is the optimal parameter
525 configuration of mSTEP, which is derived from a series of sensitivity analyses of the
526 parameters' impacts on the accuracy of the reconstructed models. As the paper shows, mSTEP
527 can be applied to both sparse and dense point clouds. The research is thus of profound
528 significance; It can help other cities or districts, which have possessed such “common” datasets
529 as topographic map and LiDAR point clouds, to produce their own BIMs/CIMs to support their
530 smart city programs.

531

532 Future research will be conducted in mainly three aspects. Firstly, the two object rectification
533 rules used in the current version of mSTEP might be too restrictive when dealing with atypical
534 architectures. Improvements thus are desired to allow reconstruction of buildings with curved
535 and irregular-shaped roofs and rooftop objects. Secondly, data from other sources, such as
536 aerial images, will be integrated with the topographic map and LiDAR point clouds to increase
537 the level of detail (*e.g.* texture) of the generated models. In this connection, other architectural
538 conventions such as symmetries or repetitive patterns should be exploited to facilitate the BIM
539 reconstruction processes.

540

541 **Acknowledgement**

542 This study is financially supported by HKU Seed Fund (201702159013) and RGC General
543 Research Fund (17201717). The assistance of the Civil Engineering and Development
544 Department (CEDD) of Hong Kong SAR in providing LiDAR point clouds for research
545 purposes is much appreciated. The authors are particularly in debt to Prof. Kincho Law at
546 Stanford University, who has spent his precious time to provide several rounds of comments
547 on the paper as it was developed. The authors would like to thank all the editors and anonymous
548 reviewers for their constructive comments.

549

550 **References**

- 551 AECbytes (2016). City Information Modeling. Available at:
552 <http://www.aecbytes.com/feature/2016/CityInformationModeling.html>, Accessed date:
553 6 January 2017.
- 554 Alexander, C., Smith-Voysey, S., Jarvis, C., and Tansey, K. (2009). Integrating building
555 footprints and LiDAR elevation data to classify roof structures and visualise buildings.

556 Computers, Environment and Urban Systems, 33(4), 285-292.
557 doi:10.1016/j.compenvurbsys.2009.01.009.

558 ASPRS (American Society for Photogrammetry & Remote Sensing). (2005). LAS
559 specification version 1.1. Available at: [http://www.asprs.org/wp-](http://www.asprs.org/wp-content/uploads/2010/12/asprs_las_format_v11.pdf)
560 [content/uploads/2010/12/asprs_las_format_v11.pdf](http://www.asprs.org/wp-content/uploads/2010/12/asprs_las_format_v11.pdf), Accessed date: 6 January 2017.

561 Awrangjeb, M., Zhang, C., and Fraser, C. S. (2013). Automatic extraction of building roofs
562 using LIDAR data and multispectral imagery. *ISPRS Journal of Photogrammetry and*
563 *Remote Sensing*, 83, 1-18. doi:10.1016/j.isprsjprs.2013.05.006.

564 Cantzler, H. (2003). Improving architectural 3D reconstruction by constrained modelling.
565 Doctoral thesis, University of Edinburgh. Available at:
566 <https://www.inf.ed.ac.uk/publications/thesis/online/IP030017.pdf>, Accessed date: 6
567 January 2017.

568 Cao, R., Zhang, Y., Liu, X., and Zhao, Z. (2017). 3D building roof reconstruction from airborne
569 LiDAR point clouds: a framework based on a spatial database. *International Journal of*
570 *Geographical Information Science*, 31(7), 1359-1380.
571 doi:10.1080/13658816.2017.1301456.

572 Cheng, L., Gong, J., Li, M., and Liu, Y. (2011). 3D building model reconstruction from multi-
573 view aerial imagery and lidar data. *Photogrammetric Engineering & Remote Sensing*,
574 77(2), 125-139. doi:10.14358/PERS.77.2.125.

575 Choi, J. O., Chen, X. B., and Kim, T. W. (2017). Opportunities and challenges of modular
576 methods in dense urban environment. *International Journal of Construction*
577 *Management*, 1-13. doi:10.1080/15623599.2017.1382093.

578 Dorninger, P., and Pfeifer, N. (2008). A comprehensive automated 3D approach for building
579 extraction, reconstruction, and regularization from airborne laser scanning point
580 clouds. *Sensors*, 8(11), 7323-7343. doi:10.3390/s8117323.

581 ESRI (2016). Lidar point classification, Available at:
582 [http://desktop.arcgis.com/en/arcmap/10.4/manage-data/las-dataset/lidar-point-](http://desktop.arcgis.com/en/arcmap/10.4/manage-data/las-dataset/lidar-point-classification.htm)
583 [classification.htm](http://desktop.arcgis.com/en/arcmap/10.4/manage-data/las-dataset/lidar-point-classification.htm), Accessed date: 15 January 2017.

584 Fischler, M. A., and Bolles, R. C. (1981). Random sample consensus: a paradigm for model
585 fitting with applications to image analysis and automated cartography.
586 *Communications of the ACM*, 24(6), 381-395. doi:10.1145/358669.358692.

587 Gilani, S. A. N., Awrangjeb, M., and Lu, G. (2016). An automatic building extraction and
588 regularisation technique using LiDAR point cloud data and Orthoimage. *Remote*
589 *Sensing*, 8(3), 258. doi:10.3390/rs8030258.

590 Goebbelsa, S., and Pohle-Fröhlich, R. (2016). Roof reconstruction from airborne laser
591 scanning data based on image processing methods. *ISPRS Annals of Photogrammetry,
592 Remote Sensing and Spatial Information Sciences*, 407-414. doi:10.5194/isprs-annals-
593 III-3-407-2016.

594 Gröger, G., and Plümer, L. (2012). CityGML–Interoperable semantic 3D city models. *ISPRS
595 Journal of Photogrammetry and Remote Sensing*, 71, 12-33.
596 doi:10.1016/j.isprsjprs.2012.04.004.

597 Haala, N., and Kada, M. (2010). An update on automatic 3D building reconstruction. *ISPRS
598 Journal of Photogrammetry and Remote Sensing*, 65(6), 570-580.
599 doi:10.1016/j.isprsjprs.2010.09.006.

600 Habib, A. F., Zhai, R., and Kim, C. (2010). Generation of complex polyhedral building models
601 by integrating stereo-aerial imagery and lidar data. *Photogrammetric Engineering &
602 Remote Sensing*, 76(5), 609-623. doi:10.14358/PERS.76.5.609.

603 Henn, A., Gröger, G., Stroh, V., and Plümer, L. (2013). Model driven reconstruction of roofs
604 from sparse LIDAR point clouds. *ISPRS Journal of Photogrammetry and Remote
605 Sensing*, 76, 17-29. doi:10.1016/j.isprsjprs.2012.11.004.

606 Henriesson, O., and Baltsavias, E. (1997) 3-D Building Reconstruction with ARUBA: A
607 Qualitative and Quantitative Evaluation. In: Gruen, A., Baltsavias, E.P., Henriesson, O.
608 (eds) *Automatic Extraction of Man-Made Objects from Aerial and Space Images (II)*.
609 Monte Verità (Proceedings of the Centro Stefano Franscini Ascona). Birkhäuser, Basel.
610 doi:10.1007/978-3-0348-8906-3_7.

611 Heo, J., Jeong, S., Park, H. K., Jung, J., Han, S., Hong, S., and Sohn, H. G. (2013). Productive
612 high-complexity 3D city modeling with point clouds collected from terrestrial LiDAR.
613 *Computers, Environment and Urban Systems*, 41, 26-38.
614 doi:10.1016/j.compenvurbsys.2013.04.002.

615 Jancosek, M., and Pajdla, T. (2011). Multi-view reconstruction preserving weakly-supported
616 surfaces. In , 2011 IEEE Conference on Computer Vision and Pattern Recognition, pp.
617 3121-3128. IEEE. doi:10.1109/CVPR.2011.5995693.

618 Javanmardi, M., Gu, Y., Javanmardi, E., Hsu, L. T., and Kamijo, S. (2015). 3D building map
619 reconstruction in dense urban areas by integrating airborne laser point cloud with 2D
620 boundary map. In 2015 IEEE International Conference on Vehicular Electronics and
621 Safety, pp. 126-131. IEEE. doi:10.1109/ICVES.2015.7396906.

622 Lafarge, F., Descombes, X., Zerubia, J., and Pierrot-Deseilligny, M. (2008). Automatic
623 building extraction from DEMs using an object approach and application to the 3D-city

624 modeling. *ISPRS Journal of Photogrammetry and Remote Sensing*, 63(3), 365-381.
625 doi:10.1016/j.isprsjprs.2007.09.003.

626 Ledoux, H., and Meijers, M. (2011). Topologically consistent 3D city models obtained by
627 extrusion. *International Journal of Geographical Information Science*, 25(4), 557-574.
628 doi:10.1080/13658811003623277.

629 Li, X., Lv, Z., Hu, J., Zhang, B., Shi, L., and Feng, S. (2015). XEarth: A 3D GIS platform for
630 managing massive city information. In 2015 IEEE International Conference on
631 Computational Intelligence and Virtual Environments for Measurement Systems and
632 Applications, pp. 1-6. IEEE. doi:10.1109/CIVEMSA.2015.7158625.

633 Li, M., Nan, L., Smith, N., and Wonka, P. (2016). Reconstructing building mass models from
634 UAV images. *Computers & Graphics*, 54, 84-93. doi:10.1016/j.cag.2015.07.004.

635 Lillesand, T., Kiefer, R. W., and Chipman, J. (2015). *Remote sensing and image interpretation*.
636 John Wiley & Sons (ISBN-13: 978-1118343289).

637 Lin, H., Gao, J., Zhou, Y., Lu, G., Ye, M., Zhang, C., Liu, L., and Yang, R. (2013). Semantic
638 decomposition and reconstruction of residential scenes from LiDAR data. *ACM*
639 *Transactions on Graphics*, 32(4), 66. doi:10.1145/2461912.2461969.

640 Mitra, N. J., and Pauly, M. (2008). Symmetry for architectural design. In *Advances in*
641 *Architectural Geometry*, 13-16. Available at:
642 [http://www0.cs.ucl.ac.uk/staff/n.mitra/research/archi_symm/paper_docs/archi_symm_](http://www0.cs.ucl.ac.uk/staff/n.mitra/research/archi_symm/paper_docs/archi_symm_agg_08.pdf)
643 [agg_08.pdf](http://www0.cs.ucl.ac.uk/staff/n.mitra/research/archi_symm/paper_docs/archi_symm_agg_08.pdf), Accessed date: 6 January 2017.

644 Musialski, P., Wonka, P., Aliaga, D. G., Wimmer, M., Gool, L. V., and Purgathofer, W. (2013).
645 A survey of urban reconstruction. *Computer Graphics Forum*, 32(6), 146-177.
646 doi:10.1111/cgf.12077.

647 Open Geospatial Consortium (2012). *OGC City Geography Markup Language (CityGML)*
648 *Encoding Standard*. Available at: <http://www.opengeospatial.org/standards/citygml>,
649 Accessed date: 6 January 2017.

650 Over, M., Schilling, A., Neubauer, S., and Zipf, A. (2010). Generating web-based 3D City
651 Models from OpenStreetMap: The current situation in Germany. *Computers,*
652 *Environment and Urban Systems*, 34(6), 496-507.
653 doi:10.1016/j.compenvurbsys.2010.05.001.

654 Peffers, K., Tuunanen, T., Rothenberger, M. A., and Chatterjee, S. (2007). A design science
655 research methodology for information systems research. *Journal of Management*
656 *Information Systems*, 24(3), 45-77. doi:10.2753/MIS0742-1222240302.

657 Poli, D., Remondino, F., Angiuli, E., and Agugiaro, G. (2015). Radiometric and geometric
658 evaluation of GeoEye-1, WorldView-2 and Pléiades-1A stereo images for 3D
659 information extraction. *ISPRS Journal of Photogrammetry and Remote Sensing*, 100,
660 35-47. doi:10.1016/j.isprsjprs.2014.04.007.

661 Poullis, C., and You, S. (2009). Automatic reconstruction of cities from remote sensor data. In
662 2009. *IEEE Conference on Computer Vision and Pattern Recognition*, pp. 2775-2782.
663 IEEE. doi:10.1109/CVPR.2009.5206562.

664 Rottensteiner, F., and Jansa, J. (2002). Automatic extraction of buildings from LIDAR data
665 and aerial images. *International Archives of Photogrammetry Remote Sensing and*
666 *Spatial Information Sciences*. Available at:
667 <http://www.isprs.org/proceedings/XXXIV/part4/pdffpapers/204.pdf>, Accessed date: 6
668 January 2017.

669 Sampath, A., and Shan, J. (2010). Segmentation and reconstruction of polyhedral building
670 roofs from aerial lidar point clouds. *IEEE Transactions on Geoscience and Remote*
671 *Sensing*, 48(3), 1554-1567. doi:10.1109/TGRS.2009.2030180.

672 Schnabel, R., Wahl, R., and Klein, R. (2007). Efficient RANSAC for point-cloud shape
673 detection. *Computer Graphics Forum*, 26(2), 214-226. doi:10.1111/j.1467-
674 8659.2007.01016.x.

675 Singh, S. P., Jain, K., and Mandla, V. R. (2014). A new approach towards image based virtual
676 3D city modeling by using close range photogrammetry. *ISPRS Annals of*
677 *Photogrammetry, Remote Sensing and Spatial Information Sciences*, 2(5), 329.
678 doi:10.5194/isprannals-II-5-329-2014.

679 Sun, S., and Salvaggio, C. (2013). Aerial 3D building detection and modeling from airborne
680 LiDAR point clouds. *IEEE Journal of Selected Topics in Applied Earth Observations*
681 *and Remote Sensing*, 6(3), 1440-1449. doi:10.1109/JSTARS.2013.2251457.

682 Tang, P., Huber, D., Akinci, B., Lipman, R., and Lytle, A. (2010). Automatic reconstruction
683 of as-built building information models from laser-scanned point clouds: A review of
684 related techniques. *Automation in Construction*, 19(7), 829-843.
685 doi:10.1016/j.autcon.2010.06.007.

686 Van Aken, J. E. (2005). Management research as a design science: Articulating the research
687 products of mode 2 knowledge production in management. *British Journal of*
688 *Management*, 16(1), 19-36. doi:10.1111/j.1467-8551.2005.00437.x.

689 Volk, R., Stengel, J., and Schultmann, F. (2014). Building Information Modeling (BIM) for
690 existing buildings—Literature review and future needs. *Automation in Construction*,
691 38, 109-127. doi:10.1016/j.autcon.2013.10.023.

692 Xiong, B., Elberink, S. O., and Vosselman, G. (2014). A graph edit dictionary for correcting
693 errors in roof topology graphs reconstructed from point clouds. *ISPRS Journal of*
694 *Photogrammetry and Remote Sensing*, 93, 227-242.
695 doi:10.1016/j.isprsjprs.2014.01.007.

696 Wu, B., Yu, B., Wu, Q., Yao, S., Zhao, F., Mao, W., and Wu, J. (2017). A graph-based
697 approach for 3D building model reconstruction from airborne LIDAR point clouds.
698 *Remote Sensing*, 9(1), 92. doi:10.3390/rs9010092.

699 Xue, F., Chen, K., Liu, D., Niu, Y., and Lu, W. (2018). An optimization-based semantic
700 building model generation method with a pilot case of a demolished construction. In:
701 Chau K., Chan I., Lu W., and Webster C. (eds) *Proceedings of the 21st International*
702 *Symposium on Advancement of Construction Management and Real Estate*. Springer,
703 Singapore. doi:10.1007/978-981-10-6190-5_22.

704 Yan, J., Jiang, W., and Shan, J. (2016). A global solution to topological reconstruction of
705 building roof models from airborne LiDAR point clouds. *ISPRS Annals of*
706 *Photogrammetry, Remote Sensing and Spatial Information Sciences*, 379-386.
707 doi:10.5194/isprs-annals-III-3-379-2016.

708 Yang, R. J., and Zou, P. X. (2016). Building integrated photovoltaics (BIPV): costs, benefits,
709 risks, barriers and improvement strategy. *International Journal of Construction*
710 *Management*, 16(1), 39-53. doi:10.1080/15623599.2015.1117709.

711 You, R. J., and Lin, B. C. (2011). A quality prediction method for building model
712 reconstruction using LiDAR data and topographic maps. *IEEE Transactions on*
713 *Geoscience and Remote Sensing*, 49(9), 3471-3480. doi:10.1109/TGRS.2011.2128326.

714 Zhang, W., Wang, H., Chen, Y., Yan, K., and Chen, M. (2014). 3D building roof modeling by
715 optimizing primitive's parameters using constraints from LiDAR data and aerial
716 imagery. *Remote Sensing*, 6(9), 8107-8133. doi:10.3390/rs6098107.

717 Zhu, L., Lehtomäki, M., Hyyppä, J., Puttonen, E., Krooks, A., and Hyyppä, H. (2015).
718 Automated 3D scene reconstruction from open geospatial data sources: Airborne laser
719 scanning and a 2D topographic database. *Remote Sensing*, 7(6), 6710-6740.
720 doi:10.3390/rs70606710.